DOI 10.1007/s11029-023-10156-0
Mechanics of Composite Materials, Vol. 59, No. 6, January, 2024

TRANSVERSE CRACK INITIATION IN THIN-PLY LAMINATES SUBJECTED TO TENSILE LOADING AT LOW AND CRYOGENIC TEMPERATURES

A. Pupurs,[1*] M. S. Loukil,[2,3] E. Marklund,[3] J. Varna[1,4] and D. Mattsson[3]

Keywords: *thin-ply laminates, cryogenic temperatures, transverse cracking, experimental testing*

Laminates with ultra-thin plies is a promising new development for polymeric composite materials expected to provide superior resistance to intralaminar crack propagation. The ply thickness effect on the crack initiation stress that according to some theoretical studies on fiber/matrix debonding does not depend on the ply thickness was investigated. Ultra-thin ply carbon fiber/epoxy cross-ply laminates subjected to tensile loading at room, –50, and –150°C temperatures relevant for cryogenic fuel storage, aeronautical, and aerospace applications were studied. The stochastic nature of the crack initiation stress in the 90°-plies was analyzed using Weibull strength distribution. The results obtained show delayed transverse crack initiation only in the thinnest plies with a clear trend that the scale parameter is much larger. This thickness effect on initiation is different than that for crack propagation which is observable in much larger ply thickness range. Regarding crack propagation, it was found that in most cases even at very high applied strain levels (1.5%) only a few transverse cracks have propagated from the specimen edges to its middle.

1. Introduction

Composite materials such as carbon fiber/epoxy laminates are increasingly used in aeronautical and aerospace applications. The use of such composites is justified by an excellent combination of their properties such as high stiffness, high strength, and low density. However, a significant limiting factor for composites in many applications is the occurrence and

[1]Laboratory of Experimental Mechanics of Materials, Riga Technical University, Riga, Latvia
[2]Division of Engineering Materials, Linköping University, Linköping, Sweden
[3]RISE Research Institutes of Sweden, Piteå, Sweden
[4]Polymeric Composites Group, Luleå University of Technology, Luleå, Sweden
[*]Corresponding author; tel.: +371 29399515; e-mail: andrejs.pupurs@rtu.lv

Original article submitted April 6, 2023; revision submitted July 27, 2023.

accumulation of micro-damage during the service life. When a multilayered composite laminate is loaded in mechanical tension with an increasing load, it will eventually fail catastrophically. The final failure, however, is usually a consequence of several micro-damage mechanisms that initiate and evolve during the loading history. The first mode of micro-damage in polymeric composites is typically the formation of transverse (intralaminar) cracks in the off-axis layers, which is followed by growth of delaminations and formation of fiber breaks in adjacent plies around the tips of the transverse cracks due to stress concentrations. The final macroscopic failure of laminate depends on the sequence and extent of the micro-damage events during the loading history. Hence, in order to improve the failure properties, safety, and general performance of composites, it is desirable to suppress the micro-damage development, especially the initiation of transverse cracks, which in most cases is the origin for development of successive damage modes. One approach to suppress the transverse crack formation is reducing the thickness of the plies in the laminate, which will effectively decrease the potential energy release rate (ERR) for the propagation of the crack along the fiber direction in the ply thus requiring higher applied load to create a tunnel-shaped crack [1-7]. Lower probability of large defects in a thin layer can also contribute to enhanced cracking resistance. Therefore, matrix cracking, delamination and splitting damage under static, fatigue, and impact loadings can be delayed without the use of special resins or through-the-thickness reinforcements. This has been proved experimentally by many studies [4-12]. In [9], unnotched strength of quasi-isotropic carbon/epoxy laminates was investigated finding that the damage onset in thin-ply quasi-isotropic laminates can be as high as 92% of the ultimate fiber failure strain level, while for conventional thickness laminates, the damage onset at 41-66% of the ultimate fiber failure strain was observed.

There are also numerous analytical and numerical studies on mechanical behavior of thin-ply laminates in the literature, e.g., [9, 12-16]. The effect of ply thickness on the crack propagation mechanisms was investigated in [4] calculating the ERR of the intralaminar transverse crack by finite element analysis. The crack suppression effect in thin ply laminates was verified concluding that this effect is caused by a decrease of the ERR at the crack tip in the thin layer. Analytical solution and closed form expressions for ERR during steady-state propagation (tunneling) of non-uniformly distributed transverse cracks in Modes I and II showing the ply thickness dependence were derived in [17].

In [14], a comprehensive review has been performed on the available analytical and numerical analysis models for predicting mechanical response and damage in thin-ply laminates. Numerical studies in [14-16] analyzed the influence of ply thickness on the so-called in-situ transverse strength and showed a significant improvement of transverse strength and delamination resistance for thin-ply laminates. The fracture mechanics based analytical models for transverse crack propagation proposed in [2, 3] have been widely implemented in analysis of transverse cracking of thin-ply laminates [9, 12-16].

However, experimental data for micro-crack evolution are usually obtained from a specimen edge observation in presence of stress magnification. Strictly speaking, the crack density observed on the specimen edge is very weakly related to the crack propagation along fibers in the ply that is ERR governed and has the ply thickness effect. As shown also in the present study, the crack density on the specimen edge in thin ply laminates may be much higher than the crack density in the bulk of the ply. The edge crack statistics describe the initiation of the crack and its propagation in ply thickness direction that after reaching critical size becomes unstable. The crack initiation is a very complex phenomenon consisting of a coalescence of growing fiber/matrix debonds through microcracks in the matrix. The stress for it to happen is different in different positions in the ply because the local stress concentrations depend on the nonuniform local fiber distribution (clustering). Hence, the crack initiation stress has a certain variation that in the present paper is described by Weibull distribution.

The ply stress level for crack initiation and its possible dependence on the ply thickness is seldom studied. There are studies in the literature, which indicate that the crack initiation stress is almost independent on the ply thickness [13, 18, 19]. In [13], computational micromechanics analysis of crack initiation through debonding (modelled using cohesive elements) and matrix yielding was performed using fiber distribution in the 90°-ply taken from optical micrographs. In [18, 19], the fiber/matrix interface crack growth dependence on the proximity of a stiff layer was analyzed showing some effect only if the debonding fiber is the closest to the ply interface.

Experimental investigation of the ply thickness effect on the initiation stress distribution is one of the objectives of the present paper.

Owing to their crack suppression ability, one useful application for thin-ply laminates could be in cryogenic fuel storage tanks for use in transport including future aerospace vehicles [20]. Thin-ply laminates could replace the existing designs of the composite fuel tanks, which utilize metallic or polymer-based liners for leakage prevention in the pressurized structure. Using the thin-ply laminates with high crack suppression ability, the liners could be omitted resulting in a more lightweight structure. Hence, it would be required to study behavior of the thin-ply laminates at low temperatures.

The present paper is focusing on analyzing the micro-cracking initiation behavior of the thin-ply laminates subjected to mechanical loading at low and cryogenic temperatures. Thin-ply cross-ply laminates made from thin continuous carbon fiber tapes provided by Oxeon, Sweden, were studied. By using different thicknesses of 90°-plies, the effect of ply thickness on density of cracks initiated at the edge was experimentally investigated at three different temperatures: room temperature (RT); –50, and –150°C and the data obtained were converted into transverse initiation stress distribution. Optical microscopy was used to quantify the transverse crack density during thermo-mechanical loading. Strain levels up to ultimate specimen failure were applied to the test specimens. The extent of propagation of the transverse cracks along the specimen width was also experimentally investigated. Weibull distribution was used to characterize the transverse initiation stress variation in plies of different thickness. Transverse ply stress for the first edge crack initiation was calculated for plies with different thicknesses. Finally, thermal cycling tests of the thin-ply laminates were performed from RT down to liquid nitrogen temperature (–196°C) to assess the possible influence of thermal cycling on crack initiation.

2. Materials and Manufacturing

In the present study, thin-ply laminates were manufactured using dry filament tape winding technique and vacuum infusion. 20-mm wide unidirectional (UD) spread tow tapes from Oxeon, Sweden, were used as filaments. The fiber type in the spread tows was Pyrofil TR50S carbon fibers from Grafil Inc. The areal weight of the spread tow tape was 50 g/m^2. Araldite LY556 epoxy resin with Aradur HY917 hardener and DY070 accelerator by Huntsman (mix ratio 100:90:0.5 by weight) were used as the matrix system. Filament winding was performed on a flat steel plate mold. To facilitate the resin flow through densely packed thin-ply fabrics, the Araldite/Aradur resin system was pre-heated to 50°C prior to starting the vacuum infusion. The temperature was held at 50°C during the resin infusion process in order to enhance resin flow. After completion of the infusion, the temperature was raised to 80°C and the laminates were cured at this temperature for 15-20 hours. After de-molding, a 4-hour long post cure cycle at 140°C was applied. Several composite plates were produced using the procedure above described.

UD composite laminates were manufactured to determine the longitudinal and transverse elastic properties of a ply. The average thickness of cured UD laminates was approximately 2 mm.

Unsymmetrical $[90_4/0_2]$ cross-ply specimens were manufactured for the purpose of experimental measurement of the difference between transverse and longitudinal thermal expansion coefficients of the UD composite, $\alpha_T - \alpha_L$, required to determine the manufacturing-induced residual stresses and the thermal stresses in plies. Procedure for determination of $\alpha_T - \alpha_L$ is described in Section 3.2.

For studying the transverse cracking in the 90°-plies symmetric cross-ply laminates were manufactured. Laminates were manufactured to study the ply thickness effect on transverse crack initiation and propagation under quasi-static loading conditions at different temperatures and for thermal cycling tests. A particular layup was designed so that several 90°-plies of different ply thicknesses were present in the same specimen and damage initiation in all plies could be studied simultaneously. Totally, 32 layers were wound on a steel plate to produce symmetric cross-ply laminates. In the manufacturing procedure of cross-ply laminates, vacuum was applied with infusion pressure of 100 mBar, and the pressure at the start of infusion was 800 mBar. The rest of the manufacturing parameters were the same as for UD specimens above described. The final average thickness of a single cured layer, t, for the cross-ply laminates was approximately equal to 50 μm. By cutting the manufactured plates in orthogonal directions, specimens corresponding to two layups were obtained: $[0_4/90_3/0_2/90/0_2/90_2/0_2]_s$ denoted as Plate A; and $[90_4/0_3/90_2/0/90_2/0_2/90_2]_s$ denoted as Plate B in the further text. For

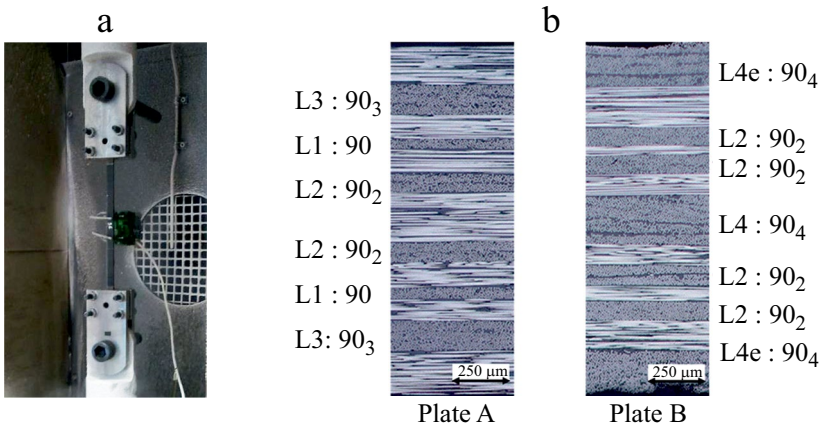

Fig. 1. (a) Typical specimen mounted in testing machine grips for testing at low temperatures, (b) typical optical microscopy images of polished cross-sections of cross-ply laminates.

Plate B, the thickest 90°-ply is the surface ply. The length of test specimens was 250 mm. Specimen ends were reinforced with glass/epoxy composite tabs in 40-mm length to enhance gripping during tensile tests. Specimen width was approximately 10 mm. Typical test specimen mounted in the testing machine grips for testing at low temperatures is shown in Fig. 1a. Optical microscopy images of typical polished edges of cross-ply laminate specimens from the Plates A and B are shown in Fig. 1b. Edge polishing was performed prior to testing. Polishing was done on a manual polishing machine using SiC papers and liquid diamond suspensions.

The 90°-plies in each laminate were denoted with respect to their thickness in terms of number of tow tape layers (see Fig. 1b): $t_{L1} \approx 50$ µm, $t_{L2} \approx 100$ µm, $t_{L3} \approx 150$ µm, and $t_{L4} \approx 200$ µm. The two of the $90°_4$ plies in Plate B are surface (external) plies; they are denoted as "L4e". It is expected that due to unconstrained surface, the transverse crack evolution in the external surface L4e-plies will be different from the internal "L4-ply" of the same thickness.

The fiber volume fraction ($V_f \approx 59\%$) of these specimens was measured using an optical image processing method with automated counting of fibers in the micrographs. Fiber area fraction was estimated by assuming an average fiber diameter of 7 µm, given in the Pyrofil TR50S carbon fiber datasheet.

3. Experimental Results

3.1. Mechanical properties

Longitudinal modulus E_L, transverse modulus E_T, and the major Poisson's ratio ν_{LT} were determined by testing 0°- and 90°-UD specimens. The UD properties were measured at room temperature (T_R) only, due to limited availability of liquid nitrogen used as coolant in the mechanical tests. The tensile tests for determining the UD properties were performed following the ASTM D3039 standard specifications [21] with an Instron 8501 test machine equipped with a 100 kN load cell. The strain was measured in both longitudinal and transverse directions with respect to the fiber direction for the 0°-specimens. For the 90°-specimens an extensometer was used to measure the strains. The longitudinal modulus E_L and Poissons's ratio ν_{LT} were determined from the recorded stress and strain data in the range between 0.05 and 0.25% axial strain. Due to the low failure strain, the transverse modulus E_T was measured between 0.05 and 0.20% of the axial strain. The measured elastic properties presented as the average values of three specimen tests are the following: $E_L = 138$ GPa, $E_T = 8.1$ GPa, $\nu_{LT} = 0.25$. Experimental values of unconstrained transverse tensile strength of the UD ply (obtained from tensile tests of 90°-specimens) were rather low, approximately 25 MPa; however, they were not used in the further study.

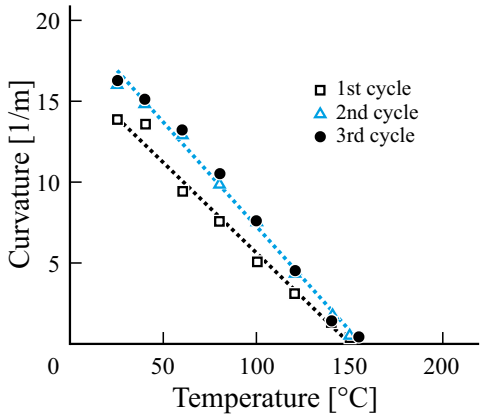

Fig. 2. Curvature as a function of temperature.

3.2. Thermal expansion coefficients

Thermal bending test of an unsymmetric $[90_4/0_2]$ cross-ply plate was used for back-calculation of the thermal expansion properties of the UD ply, which allow us to determine the manufacturing-induced residual stresses and thermal stresses in the laminate layers caused by testing temperature. At room temperature T_R, the unsymmetric specimen has a curved shape due to the residual stresses. When the specimen is heated up, the flat shape is eventually recovered, when the stress-free temperature T_{sf} is reached. In the present study, the curvature changes with respect to applied temperature were measured in three repeated heating-cooling cycles, heating the specimen until it becomes completely flat and then returning to room temperature T_R = 22°C at the end of each cycle.

The curvature dependence on temperature shown in Fig. 2 is rather linear. The curvature in the first cycle was slightly lower than in following cycles that may be explained by more relaxed residual stress in the specimen at the start of the first cycle. Nevertheless, the slope is similar as in the subsequent cycles shown in Fig. 2 where the behavior is more stable. The results of the 2nd and 3rd tests are considerable as the most relevant for low temperature conditions when the residual stress relaxation is very slow. Based on repeatability of the linear slopes determined from 2nd and 3rd cycle tests, it was assumed, that the methodology used and the values of thermal expansion coefficients obtained are representative to calculate the thermal stresses in laminate layers. Validity of this assumption is later also confirmed by good agreement of the trends in a wide range of testing temperatures as shown in Section 4.

The geometry of the curvature was estimated using standard digital image processing software with a digital ruler. The obtained relation between the curvature and the temperature and the effective stress-free temperature T_{sf} of the laminate, was used as an input in classical laminates theory (CLT) to back-calculate $\alpha_T - \alpha_L$.

In CLT, the constitutive equations for an arbitrary laminate subjected to only thermal loading are:

$$\begin{aligned} \left\{N^{th}\right\} &= [A]\{\varepsilon_0\} + [B]\{k\}, \\ \left\{M^{th}\right\} &= [B]\{\varepsilon_0\} + [D]\{k\}, \end{aligned} \tag{1}$$

where $\left\{N^{th}\right\}$ and $\left\{M^{th}\right\}$ are the thermal force and thermal moment, respectively, dependent only on the applied temperature and thermo-elastic constants of plies and laminate layup:

$$\left\{N^{th}\right\} = \Delta T \sum_{k=1}^{n} \left[\bar{Q}\right]_k \{\bar{\alpha}\}_k \left(z_k - z_{k-1}\right). \tag{2}$$

$$\left\{M^{th}\right\} = \frac{\Delta T}{2} \sum_{k=1}^{n} \left[\bar{Q}\right]_k \{\bar{\alpha}\}_k \left(z_k^2 - z_{k-1}^2\right). \tag{3}$$

$[A]$, $[B]$, and $[D]$ are the extensional, coupling, and bending stiffness matrices of laminate, respectively, $\{\varepsilon_0\}$ and $\{k\}$ are the midplane strains and curvatures of laminate, respectively, ΔT is the applied temperature change (with respect to the stress-free temperature T_{sf}), $\left[\bar{Q}\right]$ is the ply stiffness matrix in global (laminate) coordinate system, $\{\bar{\alpha}\}_k$ are the thermal expansion coefficients in global coordinate system, k is the ply number, n is the total number of plies, z_k is the interface coordinate of a ply. Solving Eq. (1) with respect to midplane curvatures $\{k\}$, a relation between the $\{k\}$ and ΔT is obtained. For a cross-ply laminate consisting of 0°- and 90°-layers, the respective thermal expansion coefficient vectors are:

$$\{\bar{\alpha}\}_0 = \begin{Bmatrix} \alpha_L \\ \alpha_T \\ 0 \end{Bmatrix} \ , \ \{\bar{\alpha}\}_{90} = \begin{Bmatrix} \alpha_T \\ \alpha_L \\ 0 \end{Bmatrix} \ , \tag{4}$$

where α_L and α_T are the longitudinal and transverse thermal expansion coefficients of the UD-ply. In the present study, it was assumed that α_L is equal to zero, since it is typically a very small entity for carbon fiber reinforced composites. Using the experimental data of temperature change ΔT and the corresponding laminate curvature $\{k\}$, and the thermo-elastic constants into Eqs (1)-(3), the transverse thermal expansion coefficient α_T can be deduced, since it is the only remaining unknown. In the present work α_T was found using the above-described CLT equations in an iterative manner, altering the value of α_T until the resulting curvatures matched with the experimentally determined values. This procedure also requires that the stress-free temperature T_{sf} is known so that the correct ΔT is being used in Eqs (2)-(3). By linear extrapolation of the experimentally measured trend between the $\{k\}$ and ΔT , it was found that the average value of T_{sf} from three heating-cooling cycles was 152°C. From the performed iterations, the average value of transverse thermal expansion coefficient α_T was determined as 27 mm/m°C.

3.3. Thermal stresses at cryogenic temperatures

In the present study micro-cracking in thin-ply composite layers at different temperatures are analyzed. While our aim is to apply a simple and robust methodology for linking the initiation of transverse cracking with the true thermal and mechanical stress level in each 90°-ply, we have tot recognize rather significant differences in thermo-elastic properties in the composites in the range between room temperature and cryogenic temperatures. As the strength and transverse stiffness is dominated by the resin and fiber-resin interface, transverse property improvement at low temperature is expected [22]. The reason for this is the reduction in polymer chain mobility, which increases the binding forces between the molecules, and therefore the strength of the material. Furthermore, according to the principle of time-temperature superposition, the lower the temperature, the more time it takes for stresses to relax, resulting in increased stiffness [22]. An increased transverse stiffness would lead to higher stresses in the 90°-plies; however, thermal stresses depend as much on the thermal expansion coefficients as they depend on the stiffness (see Eq. (2)). The dependency of transverse thermal expansion coefficient α_T on temperature is the opposite to stiffness dependence — α_T decreases with decreasing the temperature [23-25]. The literature data on dependency of stiffness and thermal expansion coefficients is somewhat limited. Since the temperature dependency of thermo-elastic properties for the used material system are not known exactly and due to the opposite effects in stiffness and thermal expansion above described, which partially cancel out the differences, we used the thermo-elastic properties determined at room temperature for calculation of the thermo-mechanical stresses at –50 and –150°C temperatures (see Section 4). As it will be shown later in Section 4, the Weibull plots for fixed ply thickness at different T versus logarithm of total stress are consistent with the assumed way of stress calculation.

Table 1 presents the calculated values of transverse stresses (sum of manufacturing-induced residual stresses and thermal stresses) for the cross-ply laminates studied prior to mechanical loading.

TABLE 1. Transverse Stresses in 90°-Layers of Cross-Ply Laminates Prior to Mechanical Loading

Temperature, °C	Transverse stress, MPa	
	Plate A	Plate B
–50	41.2	39.4
–150	61.6	58.9

3.4. Damage evolution in cross-ply laminates

Damage evolution in the cross-ply specimens subjected to tensile load was studied at T_R = 22 (room temperature), –50, and –150°C. Specimens were loaded and unloaded in steps. In each step, a certain selected maximum strain level was reached, after which the specimen was unloaded and taken out from the testing machine grips. After each loading step, the polished edges of each specimen were studied under optical microscope at T_R and the number of cracks was counted within the gage length of 50 mm in the specimen middle. No loading was applied during the inspection; however, transverse cracks were clearly visible owing to high magnification and tensile residual thermal stresses, which tend to open the crack surfaces. Thereafter, the specimens were mounted back in the testing machine and subjected to the next loading step with a higher maximum strain level (by 0.2% higher than in the previous step). The manual counting of transverse cracks was performed after each load step. All tests were performed using an Instron 8501 testing machine equipped with a 100 kN load cell. An Instron environmental chamber was used for achieving and controlling of –50 and –150°C temperatures during mechanical tests using liquid nitrogen as a coolant. When reaching the desired temperature of –50 or –150ºC, the specimens were allowed to dwell in the set temperature for 5 minutes to ensure an even temperature distribution in the specimens before starting the mechanical loading.

It was assumed that edge stress concentration effects do not have a significant influence on micro-crack evolution in different layups (Plates A and B), which have significantly different elastic moduli. This was motivated by findings in [10], where it was shown that free-edge effects are significantly suppressed in the thin-ply laminates. It was later confirmed by the experimental data obtained for L2-ply that both laminate layups give the same trends in micro-crack evolution thus excluding the influence of stress concentration at specimen edges.

The evolving transverse crack initiation in the k th 90°-ply observed at the specimen edge is characterized by the initiated crack density ρ_k^{in}, which is calculated as the number of transverse initiated transverse cracks per gage length L_g =50 mm. It is plotted with respect to the total transverse tensile stress σ_{90}^{tot} in the ply in the testing conditions. Thus, the σ_{90}^{tot} was calculated using CLT and it is a sum of mechanical stresses induced by the mechanical loading applied, residual thermal stresses at T_R, and thermal stresses induced by the temperature change from T_R to the test temperature. When analyzing results for a ply with fixed thickness, the initiated crack density data at the three test temperatures used are pooled together. The notation of plies with respect to their thickness is according to Fig. 1. The initiated crack density for L1-, L2-, L3-, and L4-plies including data for all three test temperatures is shown in Figs. 3a, 3b, 3c, and 3d, respectively.

In spite of the large scatter in Figs. 3a, b and 3c, d, the ply thickness effect on crack initiation can be directly evaluated. The crack initiation at the edge is significantly delayed only in the thinnest L1-ply. The transverse crack initiation occurs at significantly higher stress levels and the crack density at high stress is much lower than in other plies.

The trends for L2-, L3-, and L4-plies, as shown in Figs. 3, are somewhat scattered with respect to the nominal layer thickness, not showing any trend of earlier crack initiation with increasing ply thickness. In fact, the initiated crack density is the highest in L3-ply and not in the thicker L4-ply as was expected. The possible reasons for such inconsistency could be the limited amount of test specimens or the position of the L3-ply in the laminate. It is the 90°-ply, that is closest to the surface and due to limited dwelling time before the test; the temperature in this ply could be slightly lower than in the plies closer to the midplane.

The results for L4e ply are not shown because they were regarded as unrepresentative for crack initiation analysis due to presence of severe delaminations between the external L4e-ply and the neighboring 0°-ply.

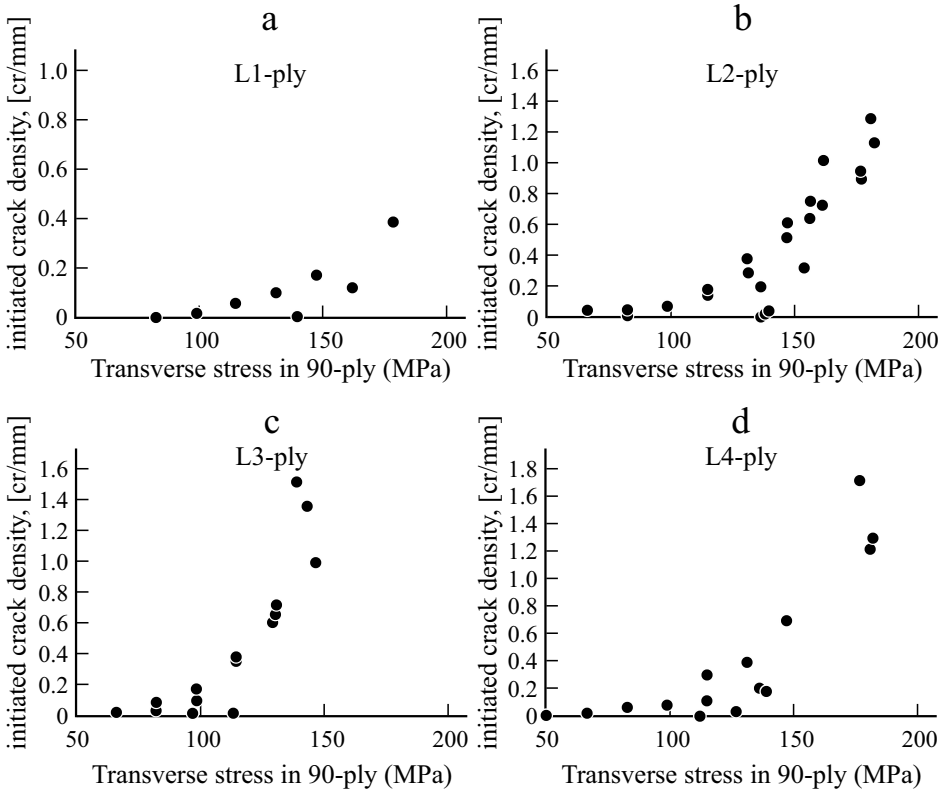

Fig. 3. Crack initiation at the specimen edge in the L1 (a), L2 (b), L3 (c), and L4 (d) 90°-plies represented by initiation crack density ρ_k^{in} vs. the calculated total thermo-mechanical transverse stress in 90°-plies according to CLT. Data for tests at T_R, –50 and –150°C are pooled in one graph: (a) ρ_{L1}^{in}, (b) ρ_{L2}^{in}, (c) ρ_{L3}^{in}, and (d) ρ_{L4}^{in}.

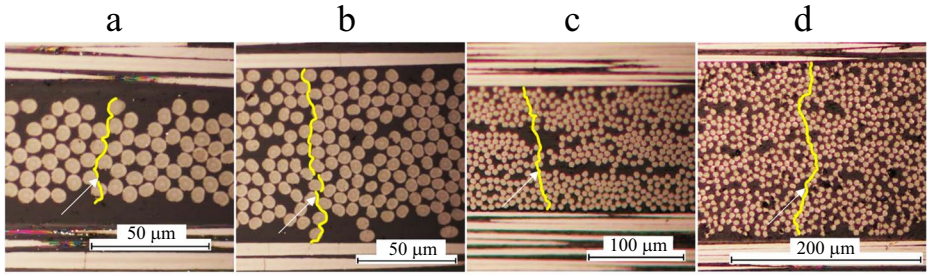

Fig. 4. Optical microscopy images of transverse cracks (highlighted for visibility) in in plies of the thin-ply laminate: (a) L1, (b) L2, (c) L3, and (d) L4.

When counting the number of initiated cracks on the polished specimen edges, only fully formed cracks spanning across the whole thickness of the ply were accounted for. Typical shape of transverse cracks in the studied 90°-plies of different thickness is presented in Fig. 4. The actual transverse cracks in Fig. 4 are highlighted for better visibility. The transverse cracks shown in Figs. 4b, 4c, and 4d correspond to L2-, L3-, and L4-plies, respectively, and they are similar to typical transverse cracks in conventional laminated composites. The transverse crack shown in Fig. 4a corresponds to the thinnest studied ply, i.e., L1-ply, with thickness being approximately equal to 50 µm. The quantification of initiated transverse cracks in the L1-ply was rather challenging as it required high optical magnification (500×) and the cracks were difficult to detect visually due to small size and small opening displacements. The crack in Fig. 4a is considered as a fully initiated transverse crack. Small cracks not spanning the whole ply thickness were disregarded in the counting procedure.

TABLE 2. Ratio between the Crack Density in the Specimen Middle ρ_k^{middle} vs the Crack Density ρ_{Lk}^{in} at the Edge of the Specimen after 1.5% Applied Strain in Tests at T_R

Plate	Layer k	$\rho_k^{middle} / \rho_k^{in}$, %
A	L3	44.9
	L2	9.3
	L1	6.7
B	L2	5.9
	L4	19.3
	L4e	38.3

Propagation of the initiated cracks leading to through-the-specimen-width tunnels (the actual crack density in the bulk of the material) was assessed by axially cutting (along the middle) several of the specimens tested at T_R. The new edges were polished and the transverse crack density denoted as ρ_k^{middle} was determined by manual counting under optical microscope. Table 2 gives the comparison between the crack density observed at the specimen edges and at the half-width of the same original specimen.

The data in Table 2 correspond to loading level of 1.5% of strain. The ratio ρ_k^{middle} / ρ_k is presented as percentage, where ρ_k is the initiated crack density measured on the specimen edges. As clearly shown in Table 2, the smaller the ply thickness, the less amount of the initiated cracks on the specimen edges have propagated to the specimen width. In fact, some of the cracks may not be the result of propagation; they could be initiated there. The data in Table 2 show that not more than 6.7% of the cracks detected on the edge of L1-ply have reached the middle of the specimen. Remarkably, even for the thicker studied layers, such as L3 and L4e, less than half of the cracks detected on the edge have propagated to the middle even after being subjected to high mechanical strains (1.5%). Transverse cracks being observed at the specimen edge and vanishing towards the middle of the specimen have also been found in [26] where X-Ray computer tomography and acoustic emission techniques were used to detect transverse cracks in thin-ply laminates.

4. Modeling Transverse Crack Initiation in Plies

In the present paper, we use the term “initiation of transverse crack” to refer to formation of through-the-thickness crack at the edge of the specimen. Hence, we define in following the crack initiation stress in a given ply as the transverse stress level, at which a complete through-the-thickness transverse crack is formed at the specimen edge.

Because of the nonuniform fiber distribution in the ply (clustering), different positions along the transverse direction of the ply have differences in local stress concentrations and, therefore, differences in resistance to crack initiation. This leads to the stochastic nature of the crack initiation stress distribution observed in a UD composite ply and the Weibull strength distribution was applied in the present study to characterize the variability. It has been shown in numerous studies, e.g., [27-30] among others, that the transverse cracking in thick 90°-plies of cross-ply polymeric composite laminates can be described by Weibull strength distribution. In thick-ply laminates the ERR for initiated crack propagation is large and, therefore, the ply stress required for propagation is lower than the one used to initiate the crack. Therefore, for thick plies with initiated cracks, the crack propagation is unstable, and the tunnel-shape crack formation stress becomes equal to the crack initiation stress.

This discussion shows that the proven applicability of the Weibull analysis for cracking in thick plies is, in fact, proof of applicability of Weibull analysis for initiation stress distribution.

The differences in crack initiation for plies of different thickness shown in Figs. 3 should lead to different Weibull parameters.

Using the Weibull theory [31] and following [28], we can consider each 90°-ply in a cross-ply laminate as a chain of elements of certain length in the transverse direction and with certain distribution of initiation stresses. If the number of

the chain elements $n \to \infty$, the cumulative probability of crack initiation P_f in the 90°-ply, when the transverse stress in the ply changes from zero to σ_T^{tot}, can be expressed as:

$$P_f = 1 - e^{-l\left(\frac{\sigma_T^{tot}}{\sigma_0}\right)^m}, \tag{5}$$

where l is the element length ratio with respect to reference length that was used to determine Weibull parameters, σ_T^{tot} is the total tensile transverse stress in the 90°-ply including the thermal residual, thermal, and mechanical stresses, σ_0 is the Weibull scale parameter for the reference element length, m is the Weibull shape parameter.

As the cross-ply specimen is loaded with incremental tensile strain ε_x, the crack was initiated first in the weakest element. In subsequent increase of the applied strain, the cracks will initiate in new elements in the same ply that is possible because of the stress transfer through the interface with the neighboring 0°-ply, and the density ρ_k^{in} of initiated cracks in the k th ply will increase. Eventually, provided that the constraining/neighboring 0°-plies stay intact, transverse crack saturation may be reached in the k th 90°-ply with $\rho_k = \rho_{k,sat}$. At transverse crack saturation, the average distance between the transverse cracks becomes critically small and the stress transfer from 0°-plies no longer can build up the stresses in the broken 90°-ply sufficient to cause new failures. Observations [27, 30] have demonstrated that this saturation length l_{sat} for polymeric composites is approximately equal to the thickness of the cracked ply. Thus, the maximum possible crack density $\rho_{k,sat}$ for each k th layer can be formulated as:

$$\rho_{k,sat} = \frac{1}{t_k} \tag{6}$$

Comparing the maximum possible crack density with experimental data in Figs. 3, we see that the crack density for all plies L_k, k = 1, 2, 3, 4 is very far from saturation and there is no need to link the element length with saturation length.

The simplest version of Weibull strength analysis assumes that the stress in the middle of an element adjacent to the one with crack is not affected by the crack. This assumption allows using in analysis the CLT stress in the ply, $\sigma_T^{tot} = \sigma_{T0}^{tot}$. That is possible only for noninteractive cracks (low crack density when the distance between cracks is about 3-5 times larger than the ply thickness). At higher crack density, the stress distribution between cracks has to be calculated. Thus, the distance between cracks for analysis to be valid has to be at least $3t_k$. It has to be noted that this condition is based on stress analysis for fully developed tunnel-shape cracks. The interaction is weaker for "freshly" initiated cracks at the edge not yet propagated along the width.

The second condition is that each element can fail only once to ensure that the element has to be sufficiently short.

The noninteractivity condition for all initiated cracks in L1-, L2-, L3-, and L4-plies in Figs. 3 is satisfied. Hence, we can select the same element length (0.05 mm is used in the present study) for all 90°-plies to obtain Weibull parameters for this reference length to perform ply thickness effect analysis on initiation stress distribution. The shape parameter does not depend on the selected element length; the scale parameter can be easily recalculated for any length of the element.

Since each element can fail only once, the maximum crack density is the same in all plies $\rho_{k,max}^{in} = 1/0.05$ cr/mm.

The probability of failure in the k th ply is defined as the number of failed elements versus the total number of elements at a given stress in the ply and can be written as:

$$P_f^k = \frac{\rho_k^{in}}{\rho_{k,max}^{in}}. \tag{7}$$

Thus, the probability of failure for each layer (Eq. (7)) can be easily obtained from the experimental data, and the Weibull parameters σ_0 and m can be extracted from Eq. (5) by plotting P_f vs. σ_{90} in double-logarithmic axes, which typically gives a linear trend

$$\ln\left[-\ln\left(1-P_f^k\right)\right] = m \cdot \ln\left(\sigma_{T0}^{tot} \Big/ \sigma_0\right). \tag{8}$$

The shape parameter m can be directly obtained as the slope of the linear trend and the scale parameter σ_0 can then be obtained from the stress-independent term in the fitting expression. The Weibull plots for all plies are shown in Fig. 5.

TABLE 3. Weibull Parameters for Plies of Different Thickness Obtained Analyzing Data at Different Temperatures

Ply	m	σ_0, MPa
L1	5.27	382.6
L2	4.54	331.7
L3	5.61	235.9
L4	4.71	321.8

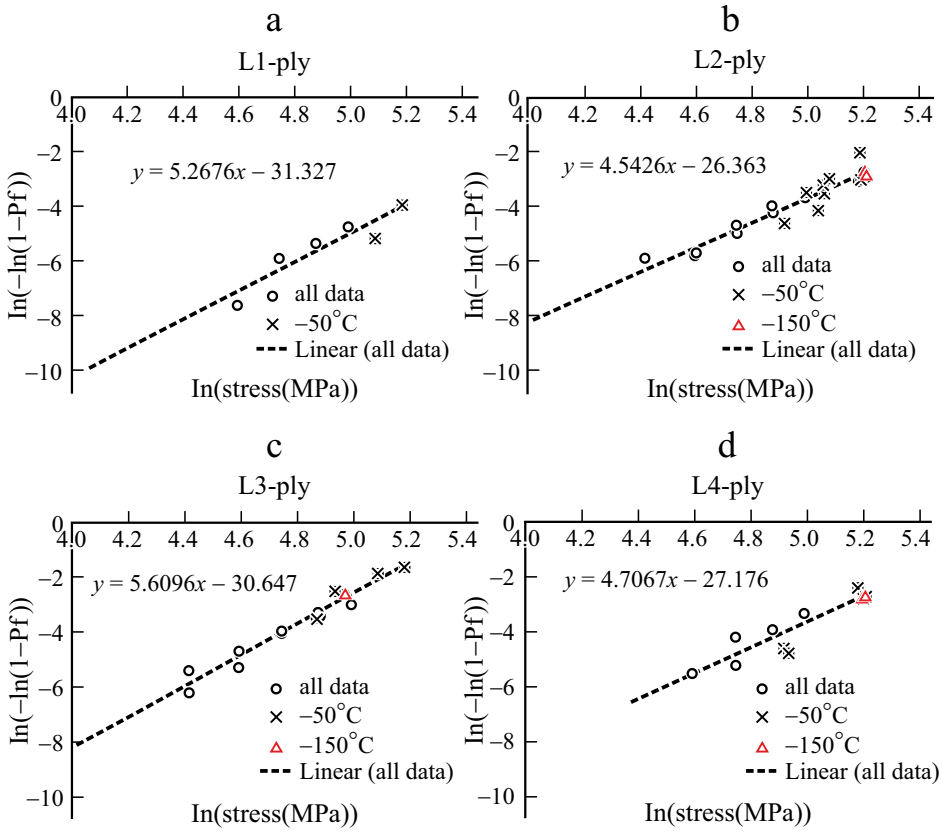

Fig. 5. Weibull plots and fitting expressions for 90°-plies in the cross-ply laminate: (a) L1, (b) L2, (c) L3, and (d) L4. Data from tests at all temperatures are presented as open symbols.

Data points corresponding to all test temperatures are shown as circular markers; the data points corresponding low temperatures (–50 and –150°C) are additionally indicated with different markers.

The Weibull parameters for all 90°-plies obtained are given in Table 3.

According to Figs. 5, the crack density data for crack initiation follow Weibull distribution (linear dependence) for all ply thicknesses analyzed separately. The data from low temperature tests with stress calculated using temperature-independent thermo-elastic constants fit very well in the same trend, giving confidence to used calculation routines.

The Weibull scale parameter σ_0 is the largest for the thinnest L1-ply, which indicates it has higher resistance to crack initiation. For the rest of plies (thicker than L1), there is no specific trend and our interpretation is that ply thickness in this range does not decrease σ_0 anymore. The σ_0 stress is the lowest for L3-ply and it is almost the same for L2- and L4-plies. Some possible reasons of this discrepancy have been briefly discussed in the Section 3.4.

The Weibull shape parameter values m in Table 3 are slightly different for plies of different thickness; however, there is no specific trend. If we assume that the fiber non-uniformity in all 90°-plies is the same and that the shape parameter

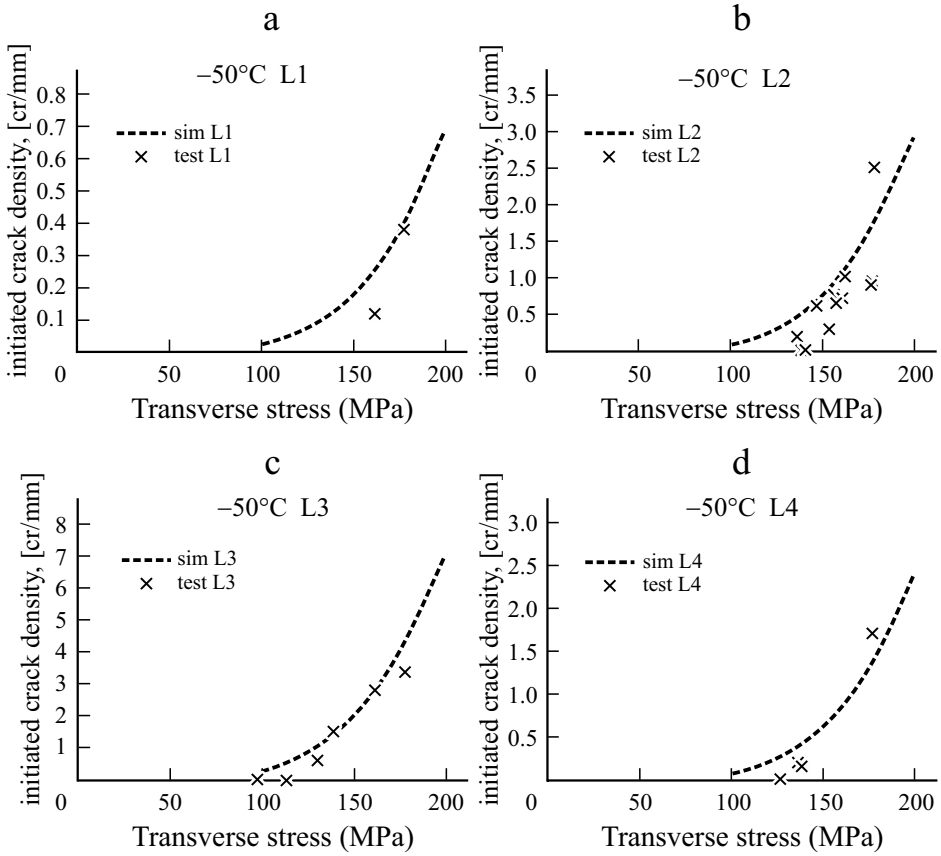

Fig. 6. Simulated and experimental initiated crack density data in tests at –50°C: (a) L1, (b) L2, (c) L3, and (d) L4.

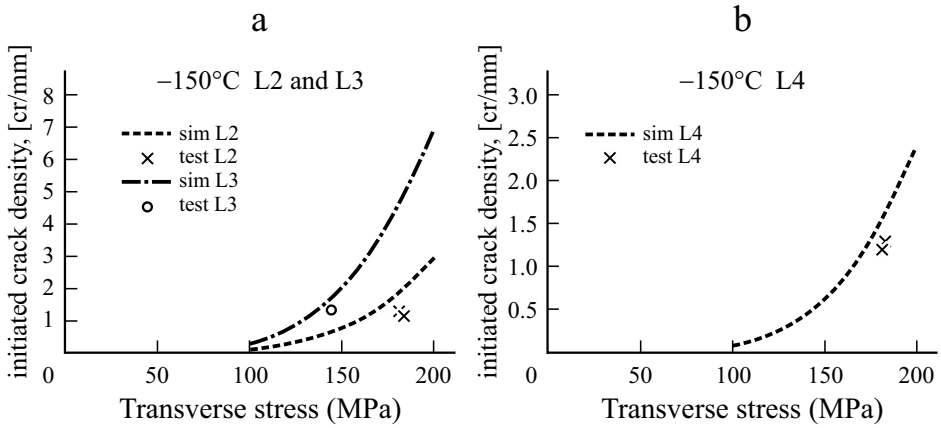

Fig. 7. Simulated and experimental initiated crack density data in tests at –150°C: (a) L2, L3 and (b) L4.

reflects it, the m variation obtained is due to insufficient amount of data points and we can use the average value $m_{av} = 5.03$. Performing new fitting of data in Fig. 5 using this m_{av}, we obtain slightly different values of the scale parameter shown in Table 4.

TABLE 4. Weibull Scale Parameter for Crack Initiation Dependence on 90°-ply Thickness, $m_{av} = 5.03$

Ply	L1	L2	L3	L4
σ_0, MPa	388.3	288.2	236.3	299.9

TABLE 5. Calculated Stress Values for First Crack Initiation over 50-mm length in Plies with Different Thickness

Ply	L1	L2	L3	L4
$\sigma^{tot}_{T\_1st}$, MPa	98.3	73.0	60.0	76.0

Nevertheless, the trends in Table 4 are the same as in Table 3: the ply resistance to crack initiation is higher only for L1-ply. So, the ply thickness effect on crack initiation stress is noticeable only for extremely thin plies. This effect on initiation does not show the square root dependence on ply thickness as it is for crack propagation. This observation agrees with theoretical investigations in [13, 18, 19].

Most of the data points in Fig. 5 used in Weibull parameter determination are from test at room temperature and only a few from low temperatures. Therefore, the applicability of parameters in Table 4 is checked by comparing predictions/simulations using Eqs. (5) and (7) with test results at –50 and –150°C presented in Figs. 6 and 7, respectively.

In spite of very large scatter typical for data at cryogenic temperatures and just a few data points, the Weibull distribution identified is fairly well describing the trends and the magnitude of intralaminar crack initiation.

Another parameter of interest in many applications, including cryogenic pressure vessels, is the stress/strain value at first ply failure. The first ply failure in composite laminates may typically be associated with very high scatter; hence, a direct comparison of the first experimental data point (first recorded crack) for each layer in the cross-ply laminates studied would not be an accurate method. Instead, we used the Weibull parameters obtained for each layer and then implemented Eq (9) that can be easy derived from Eqs. (5)-(7) to estimate the stress level $\sigma^{tot}_{T,1st}$, at which crack density ρ_c equal to $1/L_g$ (i.e. one crack per gage length $L_g = 50$ mm) is achieved:

$$\sigma^{tot}_{T,1st} = \sigma_0 \left[-\ln\left(1 - \frac{t_k}{L_g}\right)\right]^{1/m}. \tag{9}$$

The gage length $L_g = 50$ mm corresponds to the exact gage length for transverse crack inspection used in the experimental work. The first crack initiation stress values obtained are presented in Table 5.

5. Thermal Cycling

Since in the damage evolution tests (described in Section 3.4) consisted of mechanical loading at low temperatures and inspection for cracks at T_R involved several (less than 10) temperature cycles, the possible effect of thermal cycling on the crack initiation at the specimen edge was evaluated in a separate study, where mechanical load was not used and only the temperature was cycled.

Cross-ply laminate specimens from the same plates used in mechanical tests were subjected to cyclic thermal loading by submerging specimens in liquid nitrogen (temperature –196°C) and then returning them to room temperature. Specimens were submerged in liquid nitrogen (in a container) for 10 seconds, after which the specimens were taken out from the nitrogen bath and placed on a table to allow them to recover slowly back to room temperature. For handling purposes, the specimen ends were attached to metallic chains through pre-drilled holes. The set-up described allowed simultaneous cycling of multiple specimens and allowed the specimens to expand or contract freely during the thermal cycling. To speed

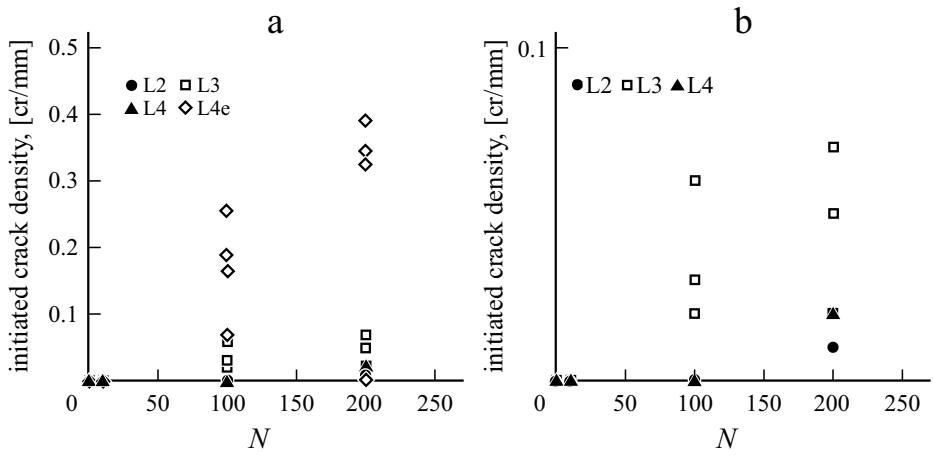

Fig. 8. Evolution of transverse cracks in laminate layers during thermal cycling: (a) all layers and (b) internal layers only.

up the recovery back to room temperature after removing the specimens from liquid nitrogen bath, a hot air gun was used positioned sufficiently far from test specimens to avoid overheating. In total 200 thermal cycles were applied and 8 specimens were tested in this experiment. Initiation of micro-damage (such as intralaminar cracks) during the thermal cycling was monitored and quantified in the 90°-plies of every specimen by performing optical microscopy inspection after 10, 100, and 200 thermal loading cycles. It was noted that after a certain amount of thermal loading cycles intralaminar cracks similar to those in the mechanical tensile tests initiate in the laminate plies at the edge. Delaminations were not found.

Evolution of transverse crack initiation in laminate plies during cyclic thermal loading is presented in Fig. 8, where the density of initiated cracks ρ_c is plotted with respect to number of applied cryogenic thermal cycles N. Data from several test specimens are presented to demonstrate the scatter between specimens. Figure 8a containing data for all plies shows much higher crack density in the surface L4e-ply, while Fig. 8b presents data for internal 90°-plies only for better clarity of trends.

Notably, no transverse cracks were found in any of the laminate plies during the first 10 loading cycles which also proves that growth of density of initiated transverse cracks reported in Section 3.4 comes from mechanical test only without any effects of thermal fatigue.

It was also observed that the highest crack density due to thermal cycling corresponds to external layers (L4e), see Fig. 8a, while the internal layers showed significantly lower crack density. It can be partially explained by more severe thermal shock in the surface ply directly after submersion; the surface layer is at lower temperature than the inside layers; thus, the stresses within it are enhanced. Comparing the crack density evolution in internal layers (see Fig. 8b), crack density ρ_c is the highest for L3-plies. Possible explanation to this result is similar as for L4e-ply; location of L3-ply is closer to the specimen surface which expectedly experiences higher thermal gradients and thermal stresses during the thermal cycling.

6. Conclusions

Recognizing two stages in development of each individual transverse crack: (a) its initiation as a result of coalescence of debonds forming matrix micro-cracks; and (b) crack propagation along fibers in the ply forming a tunnel-shaped crack; the focus in this study is on the former. Initiation of cracks was studied on the edges of thin-ply cross-ply specimens. Growth of density of the initiated cracks in tensile tests at room temperature as well as at low and cryogenic temperatures (–50 and –150°C) was studied for carbon/epoxy laminates.

The stochastic distribution of the crack initiation stress along the transverse direction of the ply was successfully described by Weibull strength distribution. For this purpose, data for a given ply thickness obtained from tests at three different temperatures were pooled together and presented versus the total thermo-mechanical stress in the ply. It was established that the experimental data follow the Weibull strength distribution very well and an increase of the Weibull scale parameter with decreasing ply thicknesses was proved. However, the effect of increasing resistance for crack initiation was observed only for the thinnest ply with 50 μm thickness, showing that this effect does not follow the square root relationship well known for crack propagation along fibers in the ply.

It was found by cutting specimens longitudinally that the crack density at the specimen edges is significantly higher than in the bulk of the composite, indicating that many cracks have initiated at the specimen edges but not propagated through the width of the specimen even at relatively high mechanical strains. This observation agrees with experimental evidence in the literature in the thin-ply laminates tested at room temperature and with earlier theoretical findings.

The stress for first crack initiation in 50-mm long region under the extensometer versus the ply thickness is higher only for the thinnest ply (50 μm), followed by a plateau region where the crack initiation stress becomes independent on the ply thickness when > 50 μm.

Acknowledgements. This work was supported by the European Regional Development Fund within the Activity 1.1.1.2 "Post-doctoral Research Aid" of the Specific Aid Objective 1.1.1 "To increase the research and innovative capacity of scientific institutions of Latvia and the ability to attract external financing, investing in human resources and infrastructure" of the Operational Programme "Growth and Employment" (No.1.1.1.2/VIAA/3/19/408). The authors would also like to acknowledge research project "Cryogenic Hypersonic Advanced Tank Technologies (CHATT)" coordinated by DLR-SART and funded by the EU within the 7th Framework Programme Theme 7 Transport. Experimental work of Mr. Hugo Scaglia is greatly acknowledged.

REFERENCES

1. A. Parvizi, K. W. Garrett, and J. E. Bailey, "Constrained cracking in glass fibre-reinforced epoxy cross-ply laminates," J. Mater. Sci., **13,** No.1, 195-201 (1978).
2. G. J. Dvorak and N. Laws, "Analysis of first ply failure in composite laminates," Eng. Fract. Mech., **25**, Nos. 5-6, 763-770 (1986).
3. G. J. Dvorak and N. Laws, "Analysis of progressive matrix cracking in composite laminates II. First ply failure," J. Compos. Mater., **21** No. 4, 309-329 (1987).
4. H. Saito, H. Takeuchi, and I. Kimpara, "Experimental evaluation of the damage growth restraining in 90° layer of thin-ply CFRP cross-ply laminates," Adv. Compos. Mater., **21**, No.1, 57-66 (2012).
5. T. Yokozeki, Y. Aoki, and T. Ogasawara, "Experimental characterization of strength and damage resistance properties of thin-ply carbon fiber/toughened epoxy laminates," Compos. Struct., **82** No. 3, 382-389 (2008).
6. R. Amacher, J. Cugnoni, J. Botsis, L. Sorensen, W. Smith, and C. Dransfeld, "Thin ply composites: Experimental characterization and modeling of size-effects,". Compos. Sci. Tech., **101**, 121-132 (2014).
7. S. Sihn, R. Y. Kim, K. Kawabe, and S.W. Tsai, "Experimental studies of thin-ply laminated composites," Compos. Sci. Tech., **67**, No. 6, 996-1008 (2007).
8. A. Wagih, P. Maimí, E. V. González, N. Blanco, J. R. S. De Aja, F. M. De La Escalera, R. Olsson, and E. Alvarez, "Damage sequence in thin-ply composite laminates under out-of-plane loading," Compos. Appl. Sci. Manuf., **87**, 66-77 (2016).
9. J. Cugnoni, R. Amacher, S. Kohler, J. Brunner, E. Kramer, C. Dransfeld, W. Smith, K. Scobbie, L. Sorensen, and J. Botsis, "Towards aerospace grade thin-ply composites: Effect of ply thickness, fibre, matrix and interlayer toughening on strength and damage tolerance," Compos. Sci. Tech., **168**, 467-477 (2018).
10. G. Guillamet, A. Turon, J. Costa, J. Renart, P. Linde, and J. A. Mayugo, "Damage occurrence at edges of non-crimp-fabric thin-ply laminates under off-axis uniaxial loading," Compos. Sci. Tech., **98**, 44-50 (2014).

11. T. Yokozeki, A. Kuroda, A. Yoshimura, T. Ogasawara, and T. Aoki. "Damage characterization in thin-ply composite laminates under out-of-plane transverse loadings," Compos. Struct., **93**, No. 1, 49-57 (2010).
12. I. G. García, J. Justo, A. Simon, and V. Mantič, "Experimental study of the size effect on transverse cracking in cross-ply laminates and comparison with the main theoretical models," Mech. Mater., **128**, 24-37 (2019).
13. M. Herráez, D. Mora, F. Naya, C. S. Lopes, C. González, and J. Llorca, "Transverse cracking of cross-ply laminates: A computational micromechanics perspective," Compos. Sci. Tech., **110**, 196-204 (2015).
14. A. Arteiro, G. Catalanotti, J. Reinoso, P. Linde, and P. P. Camanho, "Simulation of the mechanical response of thin-ply composites: from computational micro-mechanics to structural analysis," Arch. Comput. Meth. Eng., **26**, No. 5, 1445-1487 (2019).
15. P. P. Camanho, C. G. Dávila, S. T. Pinho, L. Iannucci, and P. Robinson, "Prediction of in situ strengths and matrix cracking in composites under transverse tension and in-plane shear," Compos. Appl. Sci. Manuf., **37**, No. 2, 165-176 (2006).
16. A. Arteiro, G. Catalanotti, A. R. Melro, P. Linde, and P. P. Camanho, "Micro-mechanical analysis of the in situ effect in polymer composite laminates," Compos. Struct., **116**, No.1, 827-840 (2014).
17. J. Varna, "Crack separation based models for microcracking", In: C.H. Zweben and P. Beaumont, eds. Comprehensive Composite Materials II, Vol. 2., Elsevier, (2018), pp. 192-220.
18. F. París, M. L. Velasco, and E. Correa, "The scale effect in composites: An explanation physically based on the different mechanisms of damage involved in failure," Compos. Struct., **257**, 113089 (2021).
19. L. Di Stasio, J. Varna, and Z. Ayadi, "Effect of the proximity to the 0°/90° interface on Energy Release Rate of fiber/matrix interface crack growth in the 90°-ply of a cross-ply laminate under tensile loading," J. Compos. Mater., **54**, No. 21, 3021-3034 (2020).
20. M. Sippel, "Promising roadmap alternatives for the SpaceLiner," Acta Astronautica, **66**, No. 11-12, 1652-1658 (2010).
21. ASTM D 3039-08 Standard Test Method for tensile Properties of Polymer Matrix Composite Materials, (2012).
22. Z. Sápi and R. Butler, "Properties of cryogenic and low temperature composite materials – A review," Cryogenics, **111**, 103190, (2020).
23. S. Choi and B. V. Sankar, "Micromechanical analysis of composite laminates at cryogenic temperatures," J. Compos. Mater., **40**, 1077–1091 (2006).
24. S. Usami, H. Ejima, T. Suzuki, and K. Asano, "Cryogenic small-flaw strength and creep deformation of epoxy resins," Cryogenics, **39**, 729–738 (1999).
25. S. Kanagaraj and S. Pattanayak, "Thermal expansion of glass fabric-epoxy composites at cryogenic temperatures," AIP Conference Proceedings **711**, 201 (2004).
26. S. Kohler, J. Cugnoni, R. Amacher, and J. Botsis, "Transverse cracking in the bulk and at the free edge of thin-ply composites: Experiments and multiscale modelling," Compos. Appl. Sci. Manuf., **124**,105468 (2019).
27. J. Varna, "Modelling mechanical performance of damaged laminates," J. Compos. Mater., **47**, No. 20-21, 2443-2474 (2013).
28. P. W. M. Peters, "The Strength Distribution of 90° Plies in 0/90/0 Graphite-Epoxy Laminates," J. Compos. Mater., **18**, No. 6, 545-556 (1984).
29. P. W. Manders, T. W. Chou, F. R. Jones, and J. W. Rock, "Statistical analysis of multiple fracture in 0°/90°/0° glass fibre/epoxy resin laminates," J. Mater. Sci., **18**, No. 10, 2876-2889 (1983).
30. H. Ben Kahla, Z. Ayadi, F. Edgren, A. Pupurs, and J. Varna. "Statistical model for initiation governed intralaminar cracking in composite laminates during tensile quasi-static and cyclic tests," Int. J. Fatig., **116**, 1-12 (2018).
31. W. Weibull, "A statistical distribution function of wide applicability," J. Appl. Mech., 293-297 (1951).